Improved Subfilter-Scale Models from the HATS Field Data

STEPHEN C. HATLEE*

Department of Meteorology, The Pennsylvania State University, University Park, Pennsylvania

JOHN C. WYNGAARD

Department of Meteorology, and Department of Mechanical Engineering, The Pennsylvania State University, University Park, Pennsylvania

(Manuscript received 26 October 2005, in final form 18 August 2006)

ABSTRACT

An earlier paper proposed simple rate-equation models for subfilter-scale (SFS) scalar flux and deviatoric stress in the terra incognita—that is, in numerical modeling applications where the filter (grid-mesh) scale is of the order of the scale of the turbulence. Here the physics in these models is extended and further tested against data from the Horizontal Array Turbulence Study (HATS) experiment. It is found that extensions of the SFS scalar-flux model do not appreciably improve its performance, although an advection term (which could easily be used in modeling applications) substantially and realistically increases the fluctuation level of SFS scalar flux. The addition of buoyancy and rapid-mean-shear terms to the SFS stress model does improve its performance, bringing it to the level of the scalar-flux model.

1. Introduction

When he designed what is now called large-eddy simulation (LES), Lilly (1967) specified that its grid-mesh scale lie in the inertial subrange so that the energy- and flux-containing turbulence is resolved. Even today, however, computer limitations do not always allow this resolution in atmospheric applications of LES, so the unresolved (also called subfilter-scale, or SFS) motions often carry significant kinetic energy and fluxes of momentum, heat, and advected constituents (Mason 1994; Sullivan et al. 2003; Otte and Wyngaard 2001; Bryan et al. 2003). This occurs also in fine-mesh mesoscale modeling, in a region of modeling space that Wyngaard (2004) termed the terra incognita.

As we shall show, it appears that current SFS models with a scalar eddy-diffusivity closure do not reliably represent the unresolved fluxes. Progress in SFS modeling has been hampered by the lack of observational data, but the array technique developed by Tong et al. (1998) and recently used in the Horizontal Array Turbulence Study (HATS; Sullivan et al. 2003) now allows direct measurements of SFS fluxes near the surface. Tong and colleagues have used the HATS data extensively in statistical studies of SFS fluxes and their maintenance (Chen et al. 2003, 2005; Chen and Tong 2006). In this paper, we use the HATS data to extend the study of the rate-equation models for SFS scalar flux and SFS deviatoric stress discussed by Wyngaard (2004).

2. The HATS dataset

The HATS array (Tong et al. 1998; Horst et al. 2004) consists of two horizontal rows, one directly above the other, of three-component sonic anemometers and thermometers that are aligned perpendicular to the prevailing wind direction. The array allows for the filtering of velocity and conserved-scalar fields in two directions, streamwise and lateral.

The lateral distance between the sensors, δy, can be adjusted to achieve different spatial filter widths $\Delta = 4\delta y$. In addition, the distance of the rows from the surface can be varied to get different values of z/Δ. The HATS experiment used four different array structures in order to achieve z/Δ values of 0.25, 0.5, 1.0, and 2.0. The streamwise integral scale l of the vertical velocity

* Current affiliation: AWS Truewind, Albany, New York.

Corresponding author address: John C. Wyngaard, The Pennsylvania State University, 627 Walker Building, University Park, PA 16802.
E-mail: jcw9@psu.edu

DOI: 10.1175/JAS3909.1

© 2007 American Meteorological Society

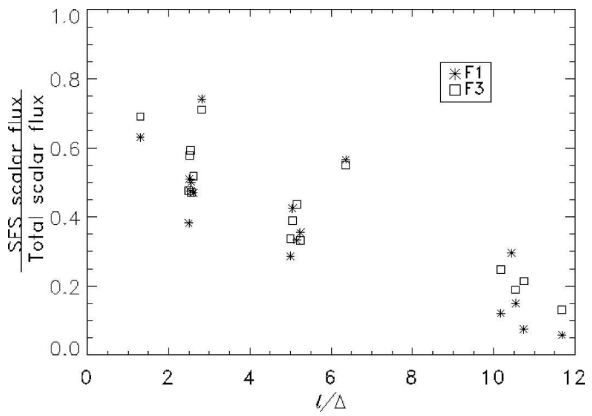

FIG. 1. The fractions of the run-averaged scalar fluxes, streamwise (f_1) and vertical (f_3), in the HATS data that are subfilter scale, from the mesoscale limit (small l/Δ) to the LES limit (large l/Δ).

near the surface is proportional to z (Kaimal et al. 1972; Peltier et al. 1996). Kaimal et al. (1972) showed using the Kansas data that $l \simeq 5z$. Thus, the HATS array provided an l/Δ range of approximately 1.25 to 10. This lies between what Wyngaard (2004) referred to as the mesoscale limit (small l/Δ; low resolution of turbulence) and the LES limit (large l/Δ; high resolution). All of the data used here were taken during the morning under unstable conditions, with z/L values around -0.2. The runs were 30 min long.

Figure 1 shows the fractions of the streamwise and vertical scalar fluxes in the HATS runs that are subfilter scale as a function of the resolution parameter l/Δ. Over the range of conditions in the runs we use here the fractions vary from about 0.7 to near 0. The scatter is due to the relatively short run length. Because of symmetry, the lateral flux averages to zero, so its values are not included.

3. Models of SFS scalar flux

The SFS flux f_i of a conserved scalar c is defined by

$$f_i = \overline{u_i c} - \overline{u}_i \overline{c}, \tag{1}$$

where an overbar represents a space average. Its evolution equation (Wyngaard 2004), generalized to include Boussinesq buoyancy effects, is

$$\frac{\partial f_i}{\partial t} + \overline{u}_j \frac{\partial f_i}{\partial x_j} + \frac{\partial}{\partial x_j}(\overline{c u_i u_j} - \overline{c u_i}\,\overline{u}_j - \overline{c}\,\overline{u_i u_j} - \overline{u}_i \overline{c u_j} + 2\overline{c}\,\overline{u}_i\,\overline{u}_j) + \frac{1}{\rho_0}\frac{\partial}{\partial x_j}(\overline{pc} - \overline{p}\,\overline{c})\delta_{ij}$$
$$= -f_j \frac{\partial \overline{u}_i}{\partial x_j} - R_{ij}\frac{\partial \overline{c}}{\partial x_j} + \frac{1}{\rho_0}\left(\overline{p\frac{\partial c}{\partial x_i}} - \overline{p}\frac{\partial \overline{c}}{\partial x_i}\right) + \frac{g}{T_0}(\overline{\theta c} - \overline{\theta}\,\overline{c})\delta_{i3}, \tag{2}$$

where p is pressure, $-R_{ij} = -\overline{u_i u_j} + \overline{u}_i \overline{u}_j$ is the SFS kinematic stress, g/T_0 is the buoyancy parameter, ρ_0 is the background density, and θ is potential temperature.

We shall call the second term on the left-hand side of Eq. (2) advection; the third, turbulent transport; and the fourth, pressure transport. The first term on the right-hand side is tilting production; the second, gradient production; the third, pressure destruction; and the fourth, buoyant production. Pressure destruction is evidently the principal rate-of-loss term (Wyngaard 2004).

a. The eddy-diffusivity model

The common use of an eddy-diffusivity SFS model for scalars in LES and mesoscale modeling is probably motivated by its simplicity and by a presumed analogy between molecular and turbulent diffusion. As shown by Wyngaard (2004), this model can also be viewed as emerging from a drastic simplification of the flux-conservation Eq. (2). The pressure-destruction term is modeled with the form originally suggested by Rotta (1951) for ensemble-mean quantities,

$$\frac{1}{\rho_0}\left(\overline{p\frac{\partial c}{\partial x_i}} - \overline{p}\frac{\partial \overline{c}}{\partial x_i}\right) \approx -\frac{f_i}{T}. \tag{3}$$

Here T is a time scale of the SFS turbulence,

$$T = C\Delta/e^{1/2}, \tag{4}$$

where Δ is the filter scale, e the SFS turbulence kinetic energy per unit mass, and C an adjustable constant. If the only other terms retained are the gradient-production terms involving the scalar gradient in the direction of the flux, Eq. (2) reduces to

$$R_{\alpha\alpha}\frac{\partial \overline{c}}{\partial x_\alpha} + \frac{f_\alpha}{T} = 0, \quad \text{no sum on } \alpha. \tag{5}$$

This yields

$$f_\alpha = -TR_{\alpha\alpha}\frac{\partial \overline{c}}{\partial x_\alpha} = -K_c\frac{\partial \overline{c}}{\partial x_\alpha}, \tag{6}$$

with K_c a scalar eddy diffusivity; that is, an eddy diffusivity that is a scalar (rather than a tensor) quantity.

As pointed out by Wyngaard (2004), the failure of

the eddy-diffusivity SFS model (6) to account for the full suite of production terms in the scalar-flux conservation Eq. (2) limits its effectiveness. This is demonstrated by Fig. 2 (bottom), which tests the predictions of Eq. (6), with C in Eq. (4) chosen as 0.3, against the HATS data. It does well for the vertical component f_3, which is due to downgradient diffusion. But it does poorly in predicting the streamwise component f_1, which is due to a combination of tilting, the neglected first term on the right-hand side of Eq. (2), and diffusion due to the vertical gradient, which is contained in the second term.

b. A simple rate-equation model

Wyngaard (2004) used the model (3) for the pressure-destruction term in Eq. (2) and retained only the time-change and the tilting- and gradient-production terms, yielding

$$\frac{\partial f_i}{\partial t} = -f_j \frac{\partial \overline{u}_i}{\partial x_j} - R_{ij} \frac{\partial \overline{c}}{\partial x_j} - \frac{f_i}{T}. \tag{7}$$

We solved Eq. (7) for f_i numerically by marching in time, determining the time-dependent parameters $\partial \overline{u}_i/\partial x_j$, R_{ij}, $\partial \overline{c}/\partial x_j$, and T from the HATS data. Figure 2 (top) shows that this simple rate–equation model (again with $C = 0.3$) does much better than the eddy-diffusivity model (6) in predicting the mean values of the SFS fluxes measured in HATS.

Its lack of an advection term causes Eq. (7) to behave improperly when the coordinate system moves at a constant velocity; such Galilean transformations are often used in LES codes. In the next section, we include advection in the equation.

c. A fuller rate-equation model

In this section we shall examine some of the terms in the SFS scalar flux Eq. (2) that are neglected by the simple rate-equation model (7). We shall include some of these terms in a fuller model of the SFS scalar budget and compare its predictions to the HATS observations.

1) HORIZONTAL ADVECTION

Wyngaard (2004) found that the streamwise advection and time-change terms were the largest pair in the SFS scalar flux evolution Eq. (2), so to leading order, that equation is

$$\frac{\partial f_i}{\partial t} + \frac{\partial \overline{u}_1 f_i}{\partial x_1} \simeq 0. \tag{8}$$

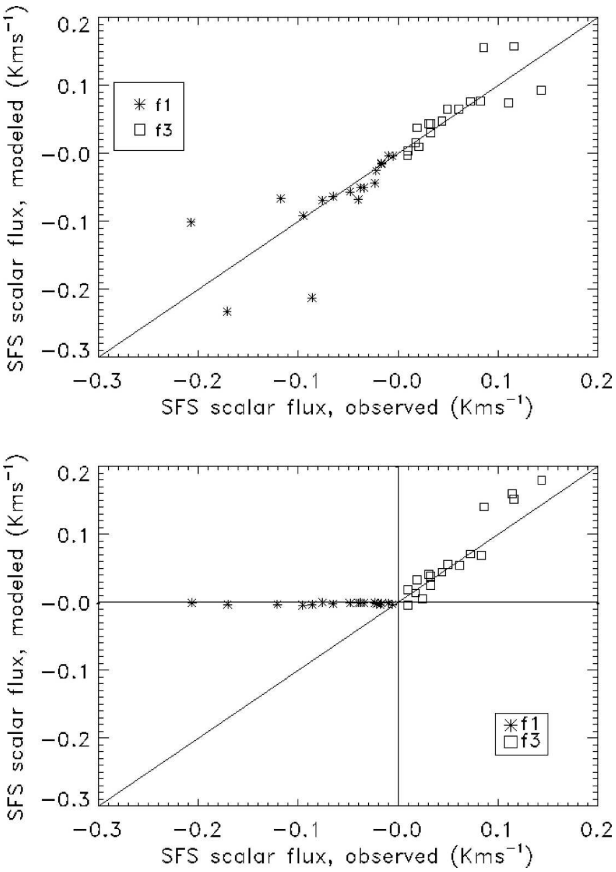

FIG. 2. Run-averaged SFS scalar flux calculated with (bottom) the eddy-diffusivity model, Eq. (6), and (top) the simple rate-equation model (7) compared to the HATS observations.

This is a version of Taylor's frozen-field hypothesis (Taylor 1938) applied to the SFS scalar flux. It also suggests that horizontal advection, being a large term, should be included in models of the SFS scalar flux equation. In principle all three components of such advection can be calculated directly when the SFS model is used within a mesoscale or LES code.

If horizontal advection is included, the simple rate-equation model (7) becomes

$$\frac{\partial f_i}{\partial t} + \frac{\partial \overline{u}_1 f_i}{\partial x_1} = -f_j \frac{\partial \overline{u}_i}{\partial x_j} - R_{ij} \frac{\partial \overline{c}}{\partial x_j} - \frac{f_i}{T}. \tag{9}$$

We can formally eliminate this horizontal advection, which was not measured in the HATS experiment, by ensemble averaging Eq. (9) and using horizontal homogeneity:

$$\frac{\partial \langle f_i \rangle}{\partial t} = -\left\langle f_j \frac{\partial \overline{u}_i}{\partial x_j} \right\rangle - \left\langle R_{ij} \frac{\partial \overline{c}}{\partial x_j} \right\rangle - \left\langle \frac{f_i}{T} \right\rangle. \tag{10}$$

We use angle brackets, $\langle\cdot\rangle$, to denote an ensemble average. If we break the turbulent variables f_i, $\overline{u}_i$, and T into ensemble-mean and fluctuating parts,

$$f_i = \langle f_i\rangle + f_i', \quad \overline{u}_i = \langle\overline{u}_i\rangle + \overline{u}_i', \quad \frac{1}{T} \equiv \omega = \langle\omega\rangle + \omega', \tag{11}$$

where ω is a frequency, Eq. (10) becomes

$$\frac{\partial\langle f_i\rangle}{\partial t} = -\langle f_j\rangle\left\langle\frac{\partial\overline{u}_i}{\partial x_j}\right\rangle - \left\langle f_j'\frac{\partial\overline{u}_i'}{\partial x_j}\right\rangle - \left\langle R_{ij}\frac{\partial\overline{c}}{\partial x_j}\right\rangle - \langle f_i\rangle\langle\omega\rangle - \langle f_i'\omega'\rangle. \tag{12}$$

This decomposition creates two unknown covariance terms, the second and fifth terms on the rhs of Eq. (12). We determined from the HATS data that these covariance terms are not negligible, so they represent a mechanism in Eq. (12) through which horizontal advection of f_i influences the mean value $\langle f_i\rangle$. Specifically, through Eq. (9), fluctuations in horizontal advection generate fluctuations in f_i, and through Eq. (12) the covariances of these f_i fluctuations and fluctuations in the resolved velocity shear and the time-scale T influence $\langle f_i\rangle$. It appears that one cannot test this by modeling the advection term in Eq. (9) with zero-mean random noise, for the mechanism requires the advection term to be correlated with the flow field. We confirmed this with numerical experiments.

A simple if crude alternative is to use Eq. (8) to model horizontal advection:

$$\frac{\partial\overline{u}_1 f_i}{\partial x_1} \approx -\left.\frac{\partial f_i}{\partial t}\right|_{\text{obs}} \equiv \left.\frac{\partial\overline{u}_1 f_i}{\partial x_1}\right|_{\text{surrogate}}. \tag{13}$$

Including this in the modeled scalar flux Eq. (7) adds a high-amplitude, chaotic, zero-mean signal that is correlated with the flow field:

$$\frac{\partial f_i}{\partial t} = -\left.\frac{\partial\overline{u}_1 f_i}{\partial x_1}\right|_{\text{surrogate}} - f_j\frac{\partial\overline{u}_i}{\partial x_j} - R_{ij}\frac{\partial\overline{c}}{\partial x_j} - \frac{f_i}{T}. \tag{14}$$

Changing the sign of the surrogate advection term in Eq. (14) should change the sign of its contribution to $\langle f_i\rangle$; we confirmed experimentally that it does.

Figure 3 shows the ratio of the run-averaged modeled SFS scalar flux calculated with the surrogate horizontal advection, Eq. (14), and without it, Eq. (7). The surrogate horizontal advection does increase the magnitude of the SFS flux by an amount that increases with l/Δ. In light of the decreasing magnitude of the SFS flux with increasing l/Δ, Fig. 1, the indicated increase in SFS flux is roughly constant at 5%–10% across the l/Δ range. This raises the possibility that an SFS model operated in an LES code in which the advection of SFS flux is computed explicitly could give different results with and without the advection term.

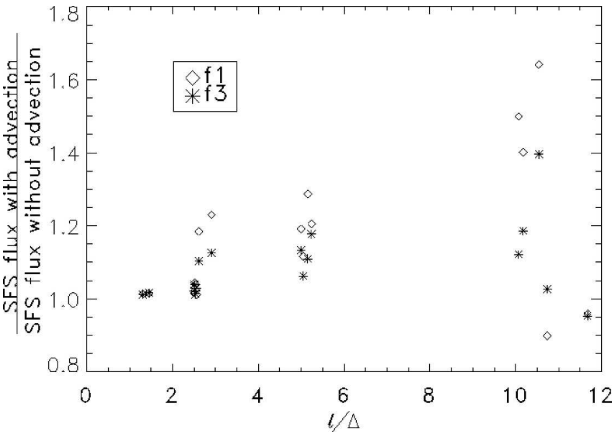

FIG. 3. Ratio of the run-averaged SFS scalar flux with surrogate advection [Eq. (14)] and without [Eq. (7)].

2) BUOYANT PRODUCTION, VERTICAL ADVECTION, AND TURBULENT TRANSPORT

Wyngaard (2004) found that in the HATS runs he analyzed the buoyant-production term in the full scalar-flux budget [Eq. (2)] contributes on average about 20% of the sum of the production terms. However, in the mesoscale limit it is as large as 40%.

Part of this buoyant-production term can, in principle, be directly removed by the pressure-destruction term because a buoyancy term also appears in the Poisson equation for pressure (Moeng and Wyngaard 1986). We will pattern our modeling here after the practice in the closure of the ensemble-mean second moment equations. Thus, we begin with the traditional decomposition of full flow variables into ensemble-mean and fluctuating parts:

$$\tilde{p} = P + p, \quad \tilde{c} = C + c, \quad \tilde{u}_i = U_i + u_i, \quad \tilde{\theta} = \Theta + \theta. \tag{15}$$

As shown by Moeng and Wyngaard (1986), the Poisson equation for the fluctuating pressure p is (neglecting the Coriolis contribution, which is negligible here):

$$\frac{1}{\rho_0}\nabla^2 p = -\left(\frac{\partial u_i}{\partial x_j}\frac{\partial u_j}{\partial x_i} - \left\langle\frac{\partial u_i}{\partial x_j}\frac{\partial u_j}{\partial x_i}\right\rangle\right) - 2\frac{\partial U_i}{\partial x_j}\frac{\partial u_j}{\partial x_i} + \frac{g}{T_0}\frac{\partial\theta}{\partial x_3}. \tag{16}$$

The first term on the right-hand side of Eq. (16) represents turbulent–turbulent interactions; it is often called the slow term. The second and third terms, which

represent mean-shear and buoyancy effects, are called rapid terms.

Following Moeng and Wyngaard (1986) we write fluctuating pressure as the sum of turbulence, mean-shear, and buoyancy parts:

$$p = p_T + p_S + p_B. \tag{17}$$

The turbulence part of pressure p_T is governed by

$$\frac{1}{\rho_0}\nabla^2 p_T = -\left(\frac{\partial u_i}{\partial x_j}\frac{\partial u_j}{\partial x_i} - \left\langle \frac{\partial u_i}{\partial x_j}\frac{\partial u_j}{\partial x_i}\right\rangle\right), \tag{18}$$

with p_S and p_B having analogous equations.

The pressure-destruction term in the scalar-flux Eq. (2) can also be written as the sum of turbulence, mean-shear, and buoyancy parts:

$$\frac{1}{\rho_0}\left(\overline{p\frac{\partial c}{\partial x_i}} - \overline{p}\frac{\partial \overline{c}}{\partial x_i}\right) \equiv \Pi_i = \Pi_i^T + \Pi_i^S + \Pi_i^B. \tag{19}$$

The simplest model of the turbulence part Π_i^T is the return-to-isotropy form

$$\Pi_i^T = -\frac{f_i}{T} \tag{20}$$

that is used in Eqs. (3) and (7).

The buoyancy part Π_i^B is typically modeled through an adjustable constant C_θ times the direct buoyant production term,

$$\Pi_i^B = -C_\theta \frac{g}{T_0}(\overline{\theta c} - \overline{\theta}\,\overline{c})\delta_{i3}, \tag{21}$$

as in Launder (1996), or with this expression with $C_\theta = \frac{1}{3}$, its value in isotropic turbulence, as in Gibson and Launder (1978) and Andrèn (1990). We follow Launder (1996) and use $C_\theta = 0.5$, so the sum of the buoyancy term and the buoyancy part of the pressure-destruction term in the modeled f_i equation is

$$\frac{g}{T_0}(\overline{\theta c} - \overline{\theta}\,\overline{c})\delta_{i3} + \Pi_i^B = (1 - C_\theta)\frac{g}{T_0}(\overline{\theta c} - \overline{\theta}\,\overline{c})\delta_{i3} = 0.5\frac{g}{T_0}(\overline{\theta c} - \overline{\theta}\,\overline{c})\delta_{i3}. \tag{22}$$

Including this buoyancy term increased the mean value of f_3 by up to 40%, with much less effect on the other components.

Wyngaard (2004) found that in the HATS data, the root-mean-square (rms) vertical advection is less than half of the rms of the total-production term, with a strong dependence on l/Δ. Thus, he also dropped the vertical advection. The vertical advection was measured in HATS so we can include it directly in our fuller rate equation.

The HATS dataset contains no data for the horizontal component of turbulent transport, which is probably small compared to horizontal advection, or for pressure transport. We do include the vertical component of turbulent transport, which yields the model

$$\frac{\partial f_i}{\partial t} + \left.\frac{\partial \overline{u}_1 f_i}{\partial x_1}\right|_{\text{surrogate}} + \overline{u}_3\frac{\partial f_i}{\partial x_3} + \frac{\partial}{\partial x_3}(\overline{cu_iu_3} - \overline{cu_i}\,\overline{u}_3 - \overline{c}\,\overline{u_iu_3} - \overline{u_i}\,\overline{cu_3} + 2\overline{c}\,\overline{u}_i\overline{u}_3)$$
$$= -f_j\frac{\partial \overline{u}_i}{\partial x_j} - R_{ij}\frac{\partial \overline{c}}{\partial x_j} + (1 - C_\theta)\frac{g}{T_0}(\overline{\theta c} - \overline{\theta}\,\overline{c})\delta_{i3} - \frac{f_i}{T}. \tag{23}$$

Equation (23) is henceforth referred to as the fuller rate-equation model.

d. Scalar-variance transfer

The evolution equation for a squared SFS scalar is (Wyngaard 2004)

$$\frac{\partial(\overline{c^2} - \overline{c}^2)}{\partial t} + \overline{u}_i\frac{\partial(\overline{c^2} - \overline{c}^2)}{\partial x_i} + \frac{\partial(\overline{u_ic^2} - \overline{u}_i\overline{c^2} - 2f_i\overline{c})}{\partial x_i} = -2\chi - 2f_i\frac{\partial \overline{c}}{\partial x_i}, \tag{24}$$

where 2χ is the rate of destruction by molecular diffusion. The last term on the right side of Eq. (24) is the rate of transfer of scalar variance from larger to smaller scales. Using the eddy-diffusivity model for f_i makes this transfer positive definite, implying that there is no backscatter; that is, the transfer of scalar variance from small scales to large scales. The fuller rate equation for f_i does allow for some backscatter, as is revealed in section 3e.

e. Fuller rate-equation model versus the HATS observations

We tested our fuller rate equation [Eq. (23)] with the HATS observations, marching it in time. We used the HATS data to determine the surrogate advection, vertical advection, and vertical turbulent transport terms on the left-hand side; the gradient-production and buoyancy terms on the right-hand side; and the param-

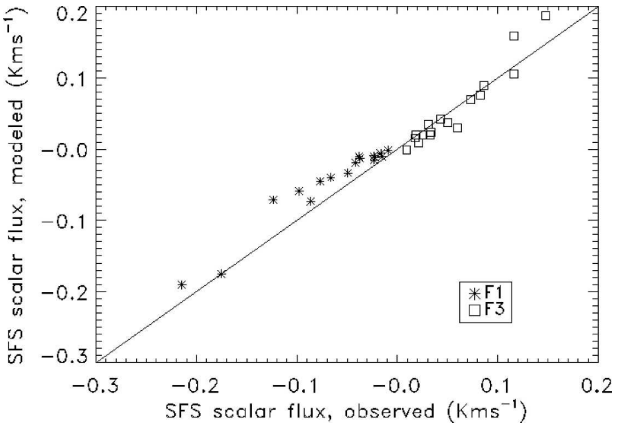

FIG. 4. Run-averaged SFS scalar fluxes calculated with the fuller rate–equation model [Eq. (23)] compared to the HATS observations.

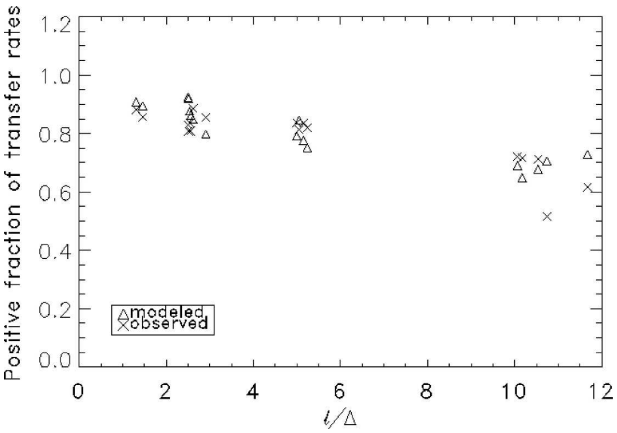

FIG. 6. The fraction of the predicted instantaneous scalar variance transfer rates that are positive compared to the HATS observations.

eters $\partial\overline{u}_i/\partial x_j$ and T. We set the constant C in the time scale, Eq. (4), at 0.21 by optimizing the agreement of the run-averaged SFS scalar fluxes and the rate of variance transfer with the HATS data.

Figure 4 compares the two components of SFS temperature fluxes from the fuller rate-equation model to the values from the HATS observations. The plot is very similar to Fig. 3 of Wyngaard (2004) but with slightly less scatter, indicating that our changes in the SFS scalar flux budget did not have a large effect on the run-averaged values of f_i. That could have significance in applications to SFS modeling in LES, where the turbulent transport term in the fuller model cannot be explicitly calculated.

Figure 5 compares the mean values of the rate of temperature-variance transfer to the HATS observations. The rates predicted by the fuller rate-equation model fit the observations well, with less scatter than the simple model of Eq. (7) [Fig. 4 of Wyngaard (2004)].

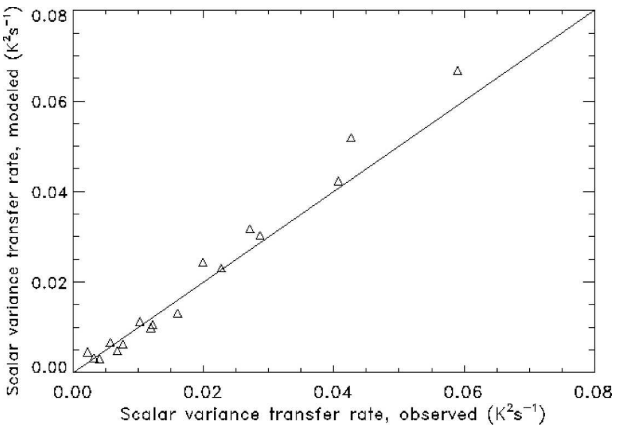

FIG. 5. Run-averaged values of the rate of scalar variance transfer compared to the HATS observations.

Figure 6 shows that the fuller rate-equation model predicts backscatter, unlike the eddy-diffusivity model. It also predicts the positive fraction of the instantaneous values of scalar variance transfer rate quite well, slightly better than Eq. (7).

Figure 7 shows time series of the measured SFS scalar flux and that from the fuller rate equation [Eq. (23)], the simple rate equation [Eq. (7)], and the eddy-diffusivity model (6). We chose a case near the mesoscale limit, where significant flux is carried by the SFS model. The inclusion of some of the terms neglected in the simpler rate equation [Eq. (7)], especially the surrogate horizontal advection, results in a time series with a higher fluctuation level. While the run-averaged values of SFS scalar flux do not change significantly, it is clear that both the eddy-diffusivity model and the simple rate-equation model underpredict its fluctuation level.

4. Models of SFS deviatoric stress

The deviatoric SFS stress is the kinematic Reynolds stress minus its isotropic form:

$$\tau_{ij} = -(\overline{u_i u_j} - \overline{u}_i\,\overline{u}_j) + \frac{2}{3}\,\delta_{ij}e = -\left(R_{ij} - \frac{2}{3}\,\delta_{ij}e\right). \tag{25}$$

The deviatoric stress has zero trace ($\tau_{ii} = 0$). The evolution equation for τ_{ij}, first derived by Lilly (1967), is[1]

[1] The form of this equation given in Wyngaard (2004) has several errors.

$$\frac{\partial \tau_{ij}}{\partial t} + \overline{u}_k \frac{\partial \tau_{ij}}{\partial x_k} = \frac{\partial}{\partial x_k}\Bigg[\overline{u_i u_j u_k} - \overline{u}_i\overline{u_j u_k} - \overline{u}_j\overline{u_i u_k} - \overline{u}_k\overline{u_i u_j} + 2\overline{u}_i\overline{u}_j\overline{u}_k - \frac{\delta_{ij}}{3}(\overline{u_l^2 u_k} - 2\overline{u}_l\overline{u_l u_k} - \overline{u_k}\,\overline{u_l^2} + 2\overline{u}_l^2\overline{u}_k)\Bigg]$$
$$+ \frac{2}{3}e\left(\frac{\partial \overline{u}_i}{\partial x_j} + \frac{\partial \overline{u}_j}{\partial x_i}\right) - \left[\tau_{ik}\frac{\partial \overline{u}_j}{\partial x_k} + \tau_{jk}\frac{\partial \overline{u}_i}{\partial x_k} - \frac{1}{3}\delta_{ij}\tau_{kl}\left(\frac{\partial \overline{u}_k}{\partial x_l} + \frac{\partial \overline{u}_l}{\partial x_k}\right)\right]$$
$$- \frac{1}{\rho}\left[\overline{p\left(\frac{\partial u_i}{\partial x_j} + \frac{\partial u_j}{\partial x_i}\right)} - \overline{p}\left(\frac{\partial \overline{u}_i}{\partial x_j} + \frac{\partial \overline{u}_j}{\partial x_i}\right)\right] + \frac{1}{\rho_0}\frac{\partial}{\partial x_k}\left[\delta_{ik}(\overline{u_j p} - \overline{u}_j\overline{p}) + \delta_{jk}(\overline{u_i p} - \overline{u}_i\overline{p})\right.$$
$$\left. - \frac{2}{3}\delta_{ij}(\overline{u_k p} - \overline{u}_k\overline{p})\right] - \frac{g}{T_0}\left[(\overline{\theta u_j} - \overline{\theta}\,\overline{u}_j)\delta_{3i} + (\overline{\theta u_i} - \overline{\theta}\,\overline{u}_i)\delta_{3j} - \frac{2\delta_{ij}}{3}(\overline{\theta u_3} - \overline{\theta}\,\overline{u}_3)\right]. \quad (26)$$

The second term on the left-hand side is advection. The terms on the right-hand side are, in order, turbulent transport, isotropic production, production by the deviatoric stress, pressure destruction, pressure transport, and buoyant production.

a. The eddy-diffusivity model

The model of τ_{ij} most commonly used in LES is the eddy-diffusivity form often referred to as the Smagorinsky model. As proposed by Lilly (1967) it stems from the truncation of Eq. (26) to two terms, isotropic production and pressure destruction, with the latter modeled as τ_{ij} divided by an SFS time scale:

$$\frac{2}{3}e\left(\frac{\partial \overline{u}_i}{\partial x_j} + \frac{\partial \overline{u}_j}{\partial x_i}\right) - \frac{\tau_{ij}}{T} = 0, \quad T = \left(\frac{3C_k}{2}\right)\frac{\Delta}{e^{1/2}}. \quad (27)$$

This gives the closure

$$\tau_{ij} = K\left(\frac{\partial \overline{u}_i}{\partial x_j} + \frac{\partial \overline{u}_j}{\partial x_i}\right), \quad K = C_k e^{1/2}\Delta. \quad (28)$$

By requiring the filter scale Δ to lie in the inertial subrange Lilly related C_k to Kolmogorov's inertial subrange spectral constant α. With the accepted value of α that yields $C_k \simeq 0.1$, the value typically used in LES (Moeng and Wyngaard 1986).

As shown in Fig. 8, upper left, the eddy-diffusivity model (28) gives $\tau_{\alpha\alpha} \simeq 0$, implying nearly equal SFS energy in the three components. The HATS observations, Fig. 8 lower, indicate that the streamwise SFS energy is larger than the average, and the vertical SFS energy smaller.

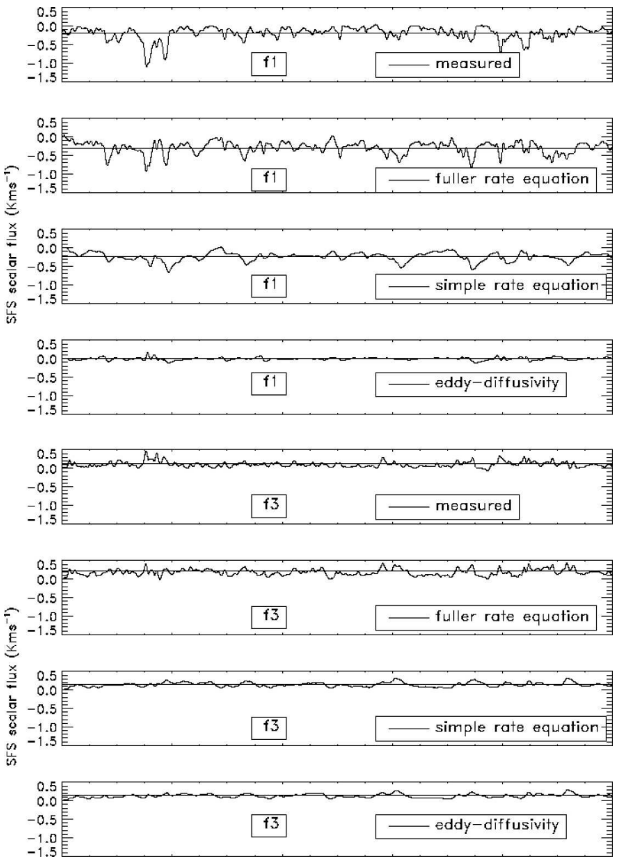

FIG. 7. Time series of SFS scalar flux from the measurements, the fuller rate Eq. (23), the simple rate Eq. (7), and the eddy-diffusivity model (6).

b. A simple rate-equation model

In addition to the two terms in Eq. (26) retained by Lilly (1967), Wyngaard (2004) retained also the local time-change and the deviatoric-production terms,

$$\frac{\partial \tau_{ij}}{\partial t} = \frac{2}{3}e\left(\frac{\partial \overline{u}_i}{\partial x_j} + \frac{\partial \overline{u}_j}{\partial x_i}\right) - \left[\tau_{ik}\frac{\partial \overline{u}_j}{\partial x_k} + \tau_{jk}\frac{\partial \overline{u}_i}{\partial x_k}\right.$$
$$\left. - \frac{1}{3}\delta_{ij}\tau_{kl}\left(\frac{\partial \overline{u}_k}{\partial x_l} + \frac{\partial \overline{u}_l}{\partial x_k}\right)\right] - \frac{\tau_{ij}}{T},$$
$$T = C_\tau \Delta/e^{1/2}, \quad (29)$$

with C_τ a constant. We shall refer to (29) as the simple rate-equation model.

The kinetic energy equation for the resolved motion,

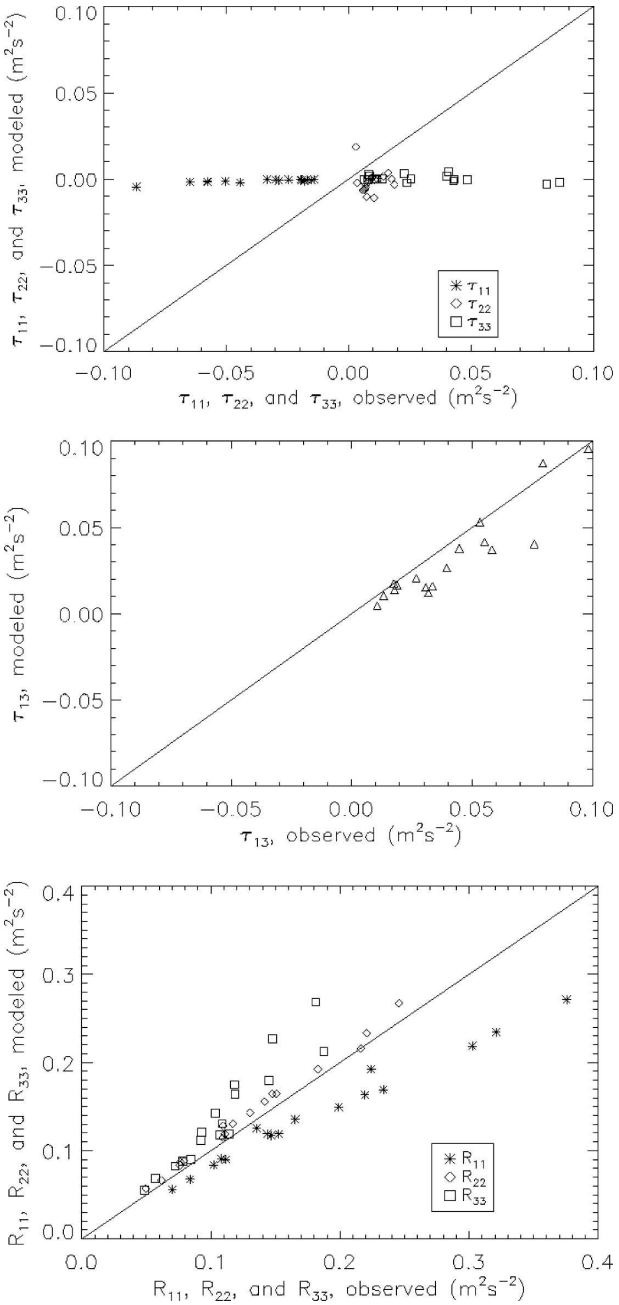

FIG. 8. Run-averaged (top) SFS deviatoric stress and (bottom) SFS variance calculated with the eddy-diffusivity model [Eq. (28)] compared to the HATS observations.

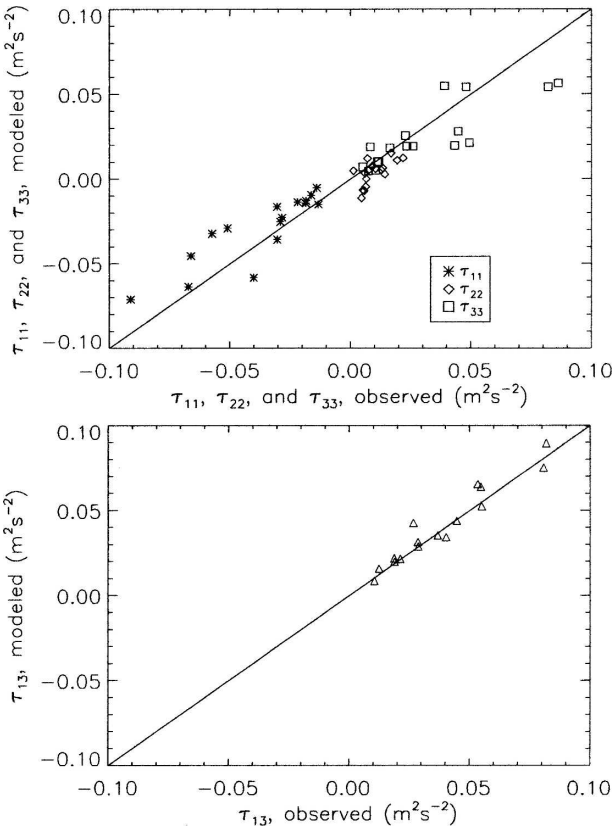

FIG. 9. Run-averaged SFS deviatoric stress calculated with the simple rate–equation model, Eq. (29), compared to the HATS observations.

which is derived by multiplying the spatially averaged Navier–Stokes equation by $\overline{u}_i$ and rearranging, is

$$\frac{\partial}{\partial t}\left(\frac{\overline{u}_i\overline{u}_i}{2}\right) + \overline{u}_j\frac{\partial}{\partial x_j}\left(\frac{\overline{u}_i\overline{u}_i}{2}\right) = -\frac{\partial}{\partial x_j}(\overline{p}^*\overline{u}_j - \overline{u}_i\tau_{ij}) - \frac{1}{2}\tau_{ij}\left(\frac{\partial\overline{u}_i}{\partial x_j} + \frac{\partial\overline{u}_j}{\partial x_i}\right) + \frac{g}{T_0}\overline{\theta}\overline{u}_3. \quad (30)$$

Here $p^* = p/\rho + 2e/3$ is a modified kinematic pressure. The second term on the rhs of Eq. (30) is a good approximation to the rate of transfer of turbulence kinetic energy from larger to smaller scales (Wyngaard 2002). As with the scalar case, using the Smagorinsky closure [Eq. (28)] makes this energy-transfer rate positive definite.

We set the constant C_τ by optimizing the run-averaged fit of τ_{ij}, Eq. (29), and the energy-transfer rate, Eq. (30), to the HATS observations. It was not possible to fit both well; Figs. 9 and 10 show the results for $C_\tau = 0.18$. The performance of the simple rate–equation model is better than the Smagorinsky model (28) but not as good as its counterpart (7) for scalar flux.

c. Inclusion of buoyancy and rapid-mean-shear terms

The inadequate performance of the simple rate-equation model (29) prompts the inclusion of a buoyancy term. Furthermore, the behavior of the SFS kinetic energy components near the surface in the HATS

experiment is suggestive of wall effects embodied in the mean-shear part of the pressure terms in the conservation equation for deviatoric stress, Eq. (26).

As shown in the appendix, our simple rate-equation model (29) extended to include buoyancy and rapid-mean-shear terms is

$$\frac{\partial \tau_{ij}}{\partial t} = \frac{2}{3} e\left(\frac{\partial \overline{u}_i}{\partial x_j} + \frac{\partial \overline{u}_j}{\partial x_i}\right) - \left[\tau_{ik}\frac{\partial \overline{u}_j}{\partial x_k} + \tau_{jk}\frac{\partial \overline{u}_i}{\partial x_k} - \frac{1}{3}\delta_{ij}\tau_{kl}\left(\frac{\partial \overline{u}_k}{\partial x_l} + \frac{\partial \overline{u}_l}{\partial x_k}\right)\right]$$
$$- \frac{g}{T_0}\left[(\overline{\theta u_j} - \overline{\theta}\overline{u}_j)\delta_{3i} + (\overline{\theta u_i} - \overline{\theta}\overline{u}_i)\delta_{3j} - \frac{2\delta_{ij}}{3}(\overline{\theta u_3} - \overline{\theta}\overline{u}_3)\right] - \frac{\tau_{ij}}{T} + \Pi_{ij}^S,$$
$$T = C_\tau \Delta / e^{1/2}, \tag{31}$$

with the rapid-mean-shear terms taken as

$$\Pi_{11}^S = -\Pi_{33}^S = -C_{11}\left(\frac{\partial U}{\partial z}\right)^2 e^{1/2}\Delta, \quad \Pi_{22}^S = 0,$$
$$\Pi_{13}^S = C_{13}\frac{\partial U}{\partial z} e. \tag{32}$$

We chose $C_\tau = 0.08$, $C_{11} = 0.4$, $C_{13} = 0.5$. The performance of this fuller rate–equation model is shown in Figs. 11–13. It predicts the mean deviatoric stress components and the mean rate of energy transfer quite well, but underestimates the amount of backscatter.

5. Summary and conclusions

Wyngaard (2004) derived simple rate-equation models for the SFS scalar flux and SFS deviatoric stress. Using data from the HATS experiment he found the model for scalar flux to be a substantial improvement over the standard eddy-diffusivity SFS model, which does not contain the flux-tilting mechanism that causes a horizontal scalar flux in the surface layer in the presence of a vertical gradient of the scalar.

We evaluated the performance of a more complete rate-equation model for the SFS scalar flux. It includes the horizontal advection, vertical advection, vertical turbulent transport, and buoyant production terms. Its performance, again evaluated with the HATS data, is not substantially better than the simple rate-equation model. We did find, however, that horizontal advection

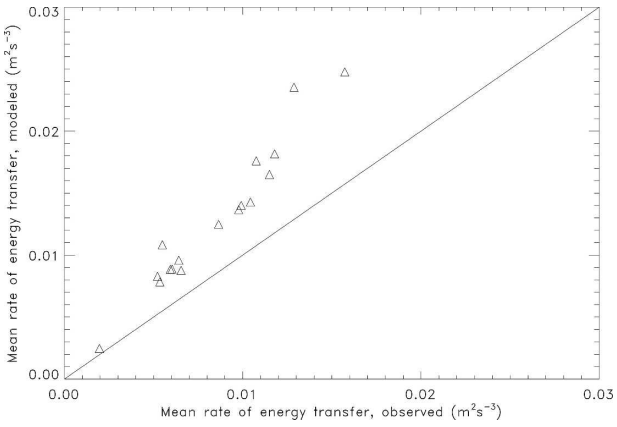

FIG. 10. Run-averaged rate of energy transfer predicted by the simple rate–equation model, Eq. (29), compared to the HATS observations.

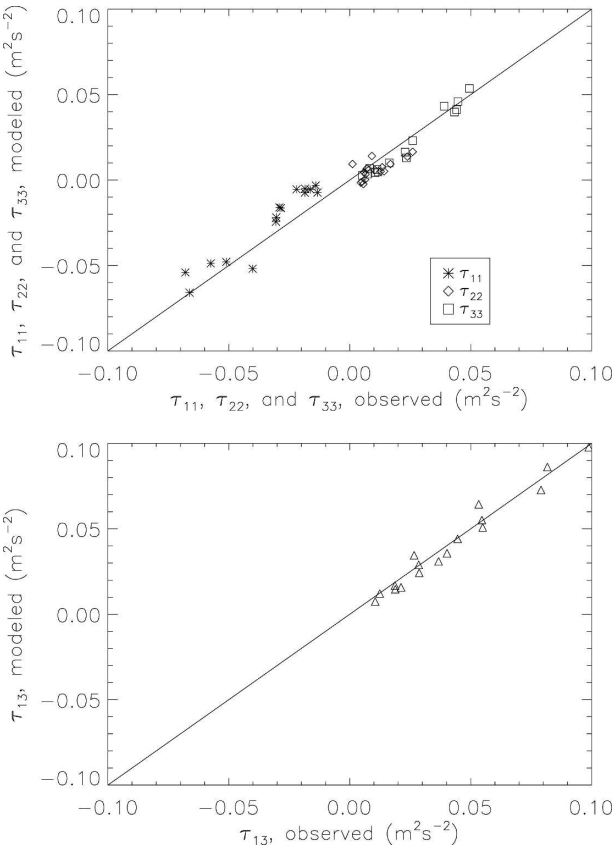

FIG. 11. Run-averaged SFS deviatoric stress calculated with the rate-equation model with rapid-mean-shear terms, Eq. (31), compared to the HATS observations.

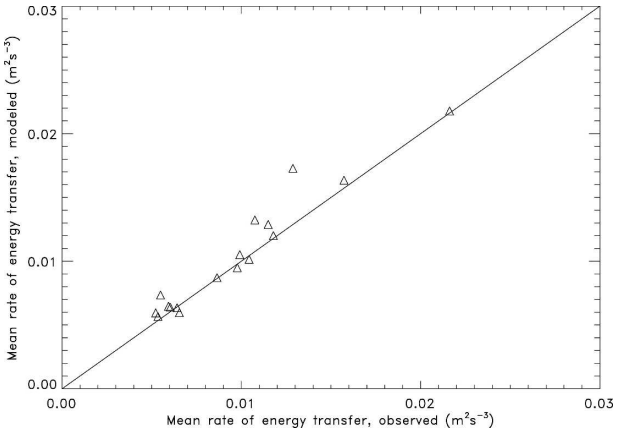

FIG. 12. Run-averaged rate of energy transfer predicted by the rate-equation model with rapid-mean-shear terms, Eq. (31), compared to the HATS observations.

of the SFS flux (as simulated with a surrogate inspired by Taylor's frozen-field hypothesis) considerably increases its local fluctuation level. We showed that through nonlinear terms in the SFS flux conservation equation this can change the mean value of SFS flux. This has implications for applications to LES and fine-mesh meteorological modeling, where advection of SFS flux can, in principle, be calculated directly.

The corresponding simple rate-equation model for SFS deviatoric stress does not perform as well. Including a rapid-mean-shear term, a model of the mean-shear contribution to the covariance representing the rate of pressure destruction of deviatoric stress, and the buoyancy term substantially improves its performance.

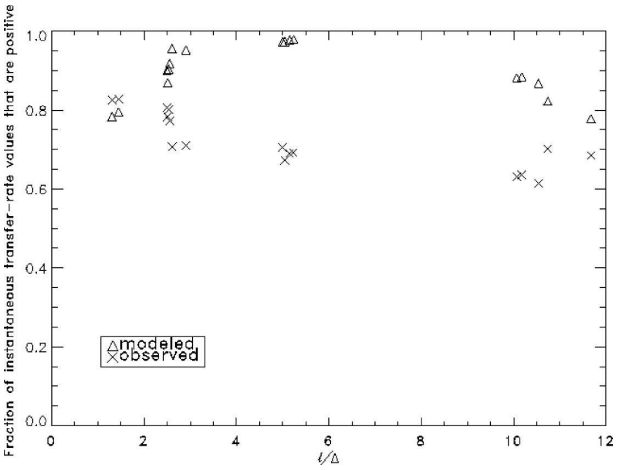

FIG. 13. The fraction of the instantaneous rate of energy transfer predictions that are positive, predicted by the rate-equation model with rapid-mean-shear terms, Eq. (31), compared to the HATS observations.

This fuller rate equation for SFS deviatoric stress clearly outperforms the standard eddy-diffusivity version.

A future array experiment that includes measurements of horizontal advection and fluctuating pressure would allow more detailed studies of the SFS flux budgets, and further testing and improving of these SFS models. In addition, longer record lengths would reduce the amount of data scatter.

Even with today's advanced state of computer technology, when the grid-mesh scale is of the order of the turbulence scale the traditional SFS models are performing outside of their intended limits; they are not designed to support a large fraction of the fluxes of scalars and momentum. Improved SFS models, such as the simple rate-equation types discussed here, offer the promise of improved modeling in this terra incognita.

Acknowledgments. This paper is based on Stephen Hatlee's master's thesis in meteorology at The Pennsylvania State University. The authors wish to thank Peter Sullivan and Tom Horst for their insightful discussions and access to the HATS data; Jingyun Wang, whose work on the 2004 paper laid the foundation for this one; and Mark Kelly and Chenning Tong, for their many helpful suggestions along the way. This work was supported in part by the National Science Foundation under Grants ATM-0222421 and ATM-0413038 and ARO Grant W911NF-04-1-0205.

APPENDIX

Rapid-Pressure Model

If we write Eq. (16) for pressure as

$$\frac{1}{\rho_0}\nabla^2 p = f(\mathbf{x}, t), \tag{A1}$$

its formal solution in a flow bounded below by a wall can be written as (Launder et al. 1975)

$$\frac{p(\mathbf{x}, t)}{\rho_0} = -\frac{1}{4\pi}\int_{\text{vol}} f(\mathbf{x}', t)\left[\frac{1}{|\mathbf{x}-\mathbf{x}'|} + \frac{1}{|\mathbf{x}-\mathbf{x}'^*|}\right] d\mathbf{x}', \tag{A2}$$

the volume of integration being the region above the wall, $x_3' > 0$. Here $\mathbf{x}'^*$ is the image of the point $\mathbf{x}'$ (i.e., its components are x_1', x_2', and $-x_3'$).

In our coordinate system aligned with the mean wind, $\partial U_i/\partial x_j = \partial U/\partial z\ \delta_{i1}\delta_{j3}$ and the Poisson equation for the mean-shear pressure p_S reads

$$\frac{1}{\rho_0}\nabla^2 p_S = -2\frac{\partial U}{\partial z}\frac{\partial u_3}{\partial x_1}. \tag{A3}$$

In view of the formal solution (A2), the exact expression for the mean-shear contribution to the pressure-strain term in Eq. (26) is

$$\Pi_{ij}^S(\mathbf{x}) = \frac{1}{2\pi}\int_{\text{vol}} \frac{\partial U(\mathbf{x}')}{\partial z} I_{ij}(\mathbf{x},\mathbf{x}') \times \left[\frac{1}{|\mathbf{x}-\mathbf{x}'|} + \frac{1}{|\mathbf{x}-\mathbf{x}'^*|}\right] d\mathbf{x}', \quad \text{(A4)}$$

where

$$I_{ij} = \frac{\partial^2}{\partial x_1' \partial x_j}(\overline{u_3' u_i} - \overline{u_3'}\,\overline{u_i}) + \frac{\partial^2}{\partial x_1' \partial x_i}(\overline{u_3' u_j} - \overline{u_3'}\,\overline{u_j}) \quad \text{(A5)}$$

is a space-averaged two-point quantity. The mean value of I_{ij} is

$$\langle I_{ij}\rangle = \frac{\partial^2}{\partial x_1' \partial x_j}\langle\overline{u_3' u_i} - \overline{u_3'}\,\overline{u_i}\rangle + \frac{\partial^2}{\partial x_1' \partial x_i}\langle\overline{u_3' u_j} - \overline{u_3'}\,\overline{u_j}\rangle, \quad \text{(A6)}$$

its principal contributions coming from resolved scales.

We use a crude simplification of Eq. (A4) for Π_{ij}^S that retains its wall-effect nature: we take the mean wind shear outside the integral, yielding

$$\Pi_{ij}^S \simeq \frac{\partial U}{\partial z}(\mathbf{x})\frac{1}{2\pi}\int_{\text{vol}} I_{ij}(\mathbf{x},\mathbf{x}')\left[\frac{1}{|\mathbf{x}-\mathbf{x}'|} + \frac{1}{|\mathbf{x}-\mathbf{x}'^*|}\right] d\mathbf{x}' = \frac{\partial U}{\partial z}(\mathbf{x}) F_{ij}, \quad \text{(A7)}$$

with F_{ij} defined by

$$F_{ij} = \frac{1}{2\pi}\int_{\text{vol}} \left[\frac{\partial^2}{\partial x_1' \partial x_j}(\overline{u_3' u_i} - \overline{u_3'}\,\overline{u_i}) + \frac{\partial^2}{\partial x_1' \partial x_i}(\overline{u_3' u_j} - \overline{u_3'}\,\overline{u_j})\right] \times \left(\frac{1}{|\mathbf{x}-\mathbf{x}'|} + \frac{1}{|\mathbf{x}-\mathbf{x}'^*|}\right) d\mathbf{x}'. \quad \text{(A8)}$$

From Eqs. (A7) and (A8) Π_{11}^S is

$$\Pi_{11}^S \simeq \frac{\partial U}{\partial z} F_{11} = \frac{\partial U}{\partial z}\frac{1}{\pi}\int_{\text{vol}} \left[\frac{\partial^2}{\partial x_1' \partial x_1}(\overline{u_3' u_1} - \overline{u_3'}\,\overline{u_1})\right] \times \left[\frac{1}{|\mathbf{x}-\mathbf{x}'|} + \frac{1}{|\mathbf{x}-\mathbf{x}'^*|}\right] d\mathbf{x}'. \quad \text{(A9)}$$

The first bracketed term in the integrand is odd in x_1, so we take it as being stress-like. We assume the mean value of the integral is proportional to the mean subfilter-scale stress $\langle uw\rangle_{\text{sfs}}$ so that

$$\Pi_{11}^S \sim \frac{\partial U}{\partial z}\langle uw\rangle_{\text{sfs}}. \quad \text{(A10)}$$

The mean subfiler-scale stress is the integral of the stress cospectrum over wavenumbers larger than $1/\Delta$ (Wyngaard and Coté 1972):

$$\langle uw\rangle_{\text{sfs}} \sim \int_{\Delta^{-1}}^{\infty} \text{Co}(\kappa)\, d\kappa \sim -\int_{\Delta^{-1}}^{\infty} \frac{\partial U}{\partial z}\epsilon^{1/3}\kappa^{-7/3}\, d\kappa \sim -\frac{\partial U}{\partial z}\epsilon^{1/3}\Delta^{4/3}. \quad \text{(A11)}$$

Taking $\epsilon \sim e^{3/2}/\Delta$ then gives

$$\Pi_{11}^S = -C_{11}\left(\frac{\partial U}{\partial z}\right)^2 e^{1/2}\Delta, \quad \text{(A12)}$$

with C_{11} a constant to be determined.

In the context of Eq. (26) for stress conservation, the rapid-mean-shear term (A12) gives

$$\frac{\partial \tau_{11}}{\partial t} + \cdots = \Pi_{11}^S + \cdots = -C_{11}\left(\frac{\partial U}{\partial z}\right)^2 e^{1/2}\Delta + \ldots \quad \text{(A13)}$$

If the constant C_{11} is positive, then the rapid-mean-shear term in Eq. (A13) is negative; thus it acts to make $\langle\tau_{11}\rangle$ negative, as observed. This represents the enhancement of SFS streamwise velocity fluctuations near the surface.

From Eqs. (A7) and (A8) Π_{13}^S is

$$\Pi_{13}^S \simeq \frac{\partial U}{\partial z}(F_{13} + F_{31}) = \frac{\partial U}{\partial z}\frac{1}{\pi}\int_{\text{vol}} \left[\frac{\partial^2}{\partial x_1' \partial x_3}(\overline{u_3' u_1} - \overline{u_3'}\,\overline{u_1}) + \frac{\partial^2}{\partial x_1' \partial x_1}(\overline{u_3' u_3} - \overline{u_3'}\,\overline{u_3})\right] \times \left[\frac{1}{|\mathbf{x}-\mathbf{x}'|} + \frac{1}{|\mathbf{x}-\mathbf{x}'^*|}\right] d\mathbf{x}'. \quad \text{(A14)}$$

The first bracketed term in the integrand is even in x_1, so we take it as being energy-like, scaling with the SFS energy e:

$$\Pi_{13}^S \sim \frac{\partial U}{\partial z} e = C_{13}\frac{\partial U}{\partial z} e, \quad \text{(A15)}$$

with C_{13} a constant to be determined.

The expression for Π_{22}^S is

$$\Pi_{22}^S \simeq \frac{\partial U}{\partial z} F_{22}$$

$$= \frac{\partial U}{\partial z} \frac{1}{\pi} \int_{\text{vol}} \left[\frac{\partial^2}{\partial x_1' \partial x_2} (\overline{u_3' u_2} - \overline{u_3'}\,\overline{u_2}) \right]$$

$$\times \left[\frac{1}{|\mathbf{x} - \mathbf{x}'|} + \frac{1}{|\mathbf{x} - \mathbf{x}'^*|} \right] d\mathbf{x}'. \qquad \text{(A16)}$$

This integral is even in x_2, so it appears to be energy-like. If we model it as of order e we have

$$\Pi_{22}^S \sim \frac{\partial U}{\partial z} e = C_{22} \frac{\partial U}{\partial z} e. \qquad \text{(A17)}$$

But this is odd in x_1, meaning that its contribution to τ_{22} changes sign with x_1; this is unphysical. It is not clear that $\langle \tau_{22} \rangle$ differs significantly from zero near the surface, and so we take $C_{22} = 0$. Thus through the zero-trace property of Π_{ij}^S we have

$$\Pi_{22}^S \simeq 0, \quad \Pi_{33}^S \simeq -\Pi_{11}^S. \qquad \text{(A18)}$$

This represents the suppression of SFS vertical velocity fluctuations near the surface.

Our simple rate-equation model (29) extended to include rapid-mean-shear terms is then

$$\frac{\partial \tau_{ij}}{\partial t} = \frac{2}{3} e \left(\frac{\partial \overline{u}_i}{\partial x_j} + \frac{\partial \overline{u}_j}{\partial x_i} \right)$$

$$- \left[\tau_{ik} \frac{\partial \overline{u}_j}{\partial x_k} + \tau_{jk} \frac{\partial \overline{u}_i}{\partial x_k} - \frac{1}{3} \delta_{ij} \tau_{kl} \left(\frac{\partial \overline{u}_k}{\partial x_l} + \frac{\partial \overline{u}_l}{\partial x_k} \right) \right]$$

$$- \frac{\tau_{ij}}{T} + \Pi_{ij}^S,$$

$$T = C_\tau \Delta / e^{1/2}, \qquad \text{(A19)}$$

with the rapid-mean-shear terms taken as

$$\Pi_{11}^S = -\Pi_{33}^S = -C_{11} \left(\frac{\partial U}{\partial z} \right)^2 e^{1/2} \Delta, \quad \Pi_{22}^S = 0,$$

$$\Pi_{13}^S = C_{13} \frac{\partial U}{\partial z} e. \qquad \text{(A20)}$$

We used $C_{11} = 0.40$, $C_{13} = 0.50$.

REFERENCES

Andrèn, A., 1990: Evaluation of a turbulence closure scheme suitable for air-pollution applications. *J. Appl. Meteor.,* **29,** 224–239.

Bryan, G. H., J. C. Wyngaard, and J. M. Fritsch, 2003: On adequate resolution for the simulation of deep moist convection. *Mon. Wea. Rev.,* **131,** 2394–2416.

Chen, Q. L., and C. N. Tong, 2006: Investigation of the subgrid-scale stress and its production rate in a convective atmospheric boundary layer using measurement data. *J. Fluid. Mech.,* **547,** 65–104.

——, H. B. Zhang, D. H. Wang, and C. N. Tong, 2003: Subgrid-scale stress and its production rate: conditions for the resolvable-scale velocity probability density function. *J. Turbul.,* **4,** 1–19.

——, D. H. Wang, H. B. Zhang, and C. N. Tong, 2005: Effects of subgrid-scale turbulence on resolvable-scale velocity-scalar statistics. *J. Turbul.,* **6,** 1–31.

Gibson, M. M., and B. E. Launder, 1978: Ground effects on pressure fluctuations in the atmospheric boundary layer. *J. Fluid Mech.,* **86,** 491–511.

Horst, T. W., J. Kleissl, D. H. Lenschow, C. Meneveau, C.-H. Moeng, M. B. Parlange, P. P. Sullivan, and J. Weil, 2004: HATS: Field observations to obtain spatially filtered turbulence fields from crosswind arrays of sonic anemometers in the atmospheric surface layer. *J. Atmos. Sci.,* **61,** 1566–1581.

Kaimal, J. C., J. C. Wyngaard, Y. Izumi, and O. R. Coté, 1972: Spatial characteristics of surface-layer turbulence. *Quart. J. Roy. Meteor. Soc.,* **98,** 563–589.

Launder, B. E., 1996: An introduction to single-point closure methodology. *Simulation and Modeling of Turbulent Flows,* T. B. Gatski et al., Eds., Oxford University Press, 243–310.

——, G. J. Reece, and W. Rodi, 1975: Progress in the development of a Reynolds-stress turbulence closure. *J. Fluid Mech.,* **68,** 537–566.

Lilly, D., 1967: The representation of small-scale turbulence in numerical simulation experiments. *Proc. IBM Scientific Computing Symp. on Environmental Sciences,* IBM, 195–210.

Mason, P. J., 1994: Large-eddy simulation: A critical review of the technique. *Quart. J. Roy. Meteor. Soc.,* **120,** 1–26.

Moeng, C.-H., and J. C. Wyngaard, 1986: An analysis of closures of pressure–scalar covariances in the convective boundary layer. *J. Atmos. Sci.,* **43,** 2499–2513.

Otte, M. J., and J. C. Wyngaard, 2001: Stably stratified interfacial-layer turbulence from large-eddy simulation. *J. Atmos. Sci.,* **58,** 3424–3442.

Peltier, L. J., J. C. Wyngaard, S. Khanna, and J. G. Brasseur, 1996: Spectra in the unstable surface layer. *J. Atmos. Sci.,* **53,** 49–61.

Rotta, J. C., 1951: Statistiche theorie nichthomogener turbulenz. *Z. Phys.,* **129,** 547–572.

Sullivan, P. P., T. W. Horst, D. H. Lenschow, C.-H. Moeng, and J. C. Weil, 2003: Structure of subfilter-scale fluxes in the atmospheric surface layer with application to large-eddy simulation modelling. *J. Fluid Mech.,* **482,** 101–139.

Taylor, G. I., 1938: The spectrum of turbulence. *Proc. Roy. Soc. London,* **164,** 476–490.

Tong, C., J. C. Wyngaard, S. Khanna, and J. G. Brasseur, 1998: Resolvable- and subgrid-scale measurement in the atmospheric surface layer: Technique and issues. *J. Atmos. Sci.,* **55,** 3114–3126.

Wyngaard, J. C., 2002: On the mean rate of energy transfer in turbulence. *Phys. Fluids,* **14,** 2426–2431.

——, 2004: Toward numerical modeling in the "terra incognita." *J. Atmos. Sci.,* **61,** 1816–1826.

——, and O. R. Coté, 1972: Cospectral similarity in the atmospheric surface layer. *Quart. J. Roy. Meteor. Soc.,* **98,** 590–603.